Authors' response to Reviewer Comment 1

Reviewer:

The Authors present and evaluate an approach to derive cloud-base height (CBH) from a network of seven upward looking all-sky imagers (ASIs). The analysis focusses on a region in NW Germany during summer and shoulder seasons. The authors demonstrate that a network approach outperforms individual pairs of ASIs.

The manuscript is generally well-written, and the figures complement the main text appropriately. I recommend publication of this article after resolving several general and few minor comments.

Authors' response:

We would like to thank the reviewer a lot for the time and effort spent on providing feedback to our manuscript and for the insightful comments. We believe that these led to valuable improvements of our manuscript. We addressed all comments and have incorporated all of the suggestions made by the reviewer as good as it was possible to us.

In the following, we will address the reviewer's further comments point-by-point. Changes are extracted from the adapted manuscript within which changes were highlighted using latexdiff. Blue indicates insertions, red indicates deletions. Please note, that the order of Sect. 3.3 and Sect. 3.4 has been reversed as suggested by General Comment 5. This change has been excluded from the markup, as it would have obscured all other changes. Further, please note, that Sect. 3 and Sect. 4 have been reworked strongly, based on Reviewer Comment 2, Major Comments 1, 2.

Changes in manuscript:

See below.

General comment 1:

The Authors motivate their work as it allows to better nowcast downwelling solar fluxes (e.g., for photovoltaic power plants) and it is said that "accurate knowledge of CBH is required". It is not perfectly obvious why better knowledge of CBH itself improves nowcasting. I'm assuming CBH is only one piece of information - apart from knowledge of each cloud's horizontal extend, cloud-top height, and geolocation (derived from satellite?) as well as the wind vector in cloudy altitudes (from meteorological forecasts or from ASIs?). Section 1 (ll. 26-32, ll. 48-53) touches on this topic but leaves open questions of how exactly this work fits into a larger picture. It is also unclear to me if voxel carving (ll. 58-59) is a competing approach or if this work could be used for voxel carving efforts – the Authors should clarify this in Section 1.

Authors' response:

We agree with the reviewer, that indeed nowcasting of solar irradiance is a complex task which includes a number of subtasks, which may all bring uncertainties to the method. Based on previous works, e.g.

Nouri, B., S. Wilbert, P. Kuhn, N. Hanrieder, M. Schroedter-Homscheidt, A. Kazantzidis, L. Zarzalejo, P. Blanc, S. Kumar and N. Goswami (2019). "Real-Time Uncertainty Specification of All Sky Imager Derived Irradiance Nowcasts." Remote Sensing **11**(9): 1059.,

knowledge of CBH was identified as critical, especially if the accurate position of cloud edges is of interest. We addressed this by a summary of the nowcasting procedure, pointing out the importance of cloud base height (CBH).

We also added a short explanation on the relationship of stereoscopic and voxel carving approaches. From our perspective these approaches are in principle competing. However, previous works have shown that voxel carving approaches can be improved, if CBH is received from a stereoscopic approach.

Changes in manuscript:

p. 3, ll. 76-78:

here (Nouri et al., 2019a) enhances the approach by Kuhn et al. (2018b) and works completely independently from cloud recognition which is considered to bring a greater robustness. While stereoscopic and voxel carving/ tomographic approaches are in principle competing techniques, Nouri et al. (2019a) demonstrated, that voxel carving-based cloud modelling can be enhanced by incorporating CBH from a stereoscopic procedure.

p.4 ll. 91-102:

The selected ASIs are located in the city of Oldenburg. At the moment of writing, Eye2Sky contains 24 ASIs in Oldenburg and a region of about 110 km × 100 km to the west of Oldenburg. ~~An approach is presented to measure CBHby the ASI network that allows the use of~~ Eye2Sky is mainly dedicated to nowcasting of solar irradiance at high spatial and temporal resolution. The forecasting procedure, which will be described in more detail in a future publication, first recognizes clouds from the images of the ASIs. Cloud observations are then projected into a horizontal plane at the current CBH. These georeferenced cloud observations of multiple ASIs are merged and cloud properties are estimated. The angular velocities of clouds, as recognized by the individual ASIs, are transformed into absolute velocities over ground relying on an accurate estimation of CBH. Clouds are tracked along received cloud motion vectors to predict the clouds' future positions. Prior works studying ASI-based forecasting systems with up to four cameras (e.g. Nouri et al., 2019b) suggested that CBH is an essential component when predicting maps of solar irradiance based on cloud observations from ASIs, as the current and future positions of cloud shadows on the ground can only be predicted accurately if the clouds' height and velocity are determined accurately. Thus, in this publication an important component of this nowcasting system, namely the estimation of CBH, is presented. Our approach allows to use multiple ASI-pairs ~~in proximity simultaneously~~organized as ASI network and located in proximity, to estimate CBH. 42 ASI-pairs are formed from the seven ASIs and CBH is estimated by each ASI-pair based on the method presented by Nouri

General comment 2:

Reviewer:

When using a network of ASIs over an area of (100km)2 to obtain a single CBH, do the Authors inherently assume a cloud (or a field of clouds) of unique base height? The Authors should make this more explicit (perhaps in Section 3) and discuss the realism of this assumption (perhaps in Section 4.4)

Authors' response:

We share the reviewer's opinion that the use of CBH assessed in the urban area for the whole region of Eye2Sky measuring 100 km x 100 km is a strong simplification. We now tried to outline, which scope our method may fulfill and how the method can be enhanced for a broader scope in future. For this, we added an explanation to Sect. 3.2, as in this section the conditions at the studied site are analyzed. More precisely our expectation from the conditions on site is, that our method is suited to provide an estimation of CBH which is useful to nowcast solar irradiance in the urban area of Oldenburg. For the task of providing nowcasts for the whole of Eye2Sky, we intend to classify the cloud conditions at larger distances from the urban area by a number of ASIs which are dispersed over the region and then to assign CBH from the urban area, by looking up which CBH was observed recently in the urban area for similar cloud conditions.

Changes in manuscript:

p. 12, ll. 305-310:

characteristics are expected to cause greater temporal and spatial variability of CBH. To conclude, a procedure, which estimates CBH of the cloud layer most dominant in the urban area of Oldenburg accurately, is considered beneficial to assess and model clouds in the same area (depicted in Fig. 1, right). Still, if clouds over the whole region covered by Eye2Sky (depicted in Fig. 1, left) are assessed, this method alone may not be sufficient. In the future, local cloud conditions may be classified by image processing techniques (e.g. Fabel et al., 2021) and CBH may be assigned to local clouds from clouds of the same type, which were recently observed in the urban area.

General comment 3:

Reviewer:

To obtain CBH probabilities (Section 3.3) the Authors use a subset of available datapoints. It is unclear what portion of the data was excluded. Did this selection mostly affect samples of high-altitude clouds? Perhaps the Authors could add a column to Table 1 that lists the fraction of data points excluded per altitude group?

Authors' response:

First of all, we would like to apologize as a statement in the manuscript was misleading. The filter excluding variable situations is applied in the modelling of conditional probabilities (now Sect. 3.4) and in Sect. 4.4 to compare performance metrics from ASI-pairs and ASI network. In Sect. 4.1-4.3 this filter is not applied.

As suggested, we added a column to Table 1, indicating the excluded fraction of time stamps per interval of CBH and added a description, how the filter influences the distribution of CBH in the validation data set. The filter excludes observations from all ranges of CBH in a similar way. However, for the lowest range of CBH a larger fraction is excluded. As this range is still represented by a large number of observations in the filtered data set, this was accepted.

Changes in manuscript:

Description on filtering of validation data was corrected, moved; additional description of the filter effect added (Sect. 4.4):

pp. 20-21, ll. 531-535:

530 from 30 June 2019 to 27 September 2019. This dataset was excluded from the model development described in Sect. 3. The analyzed quantity is 10 min-median CBH. ~~The evaluations are restricted to times in which the variability of CBH is small. More precisely, the standard deviation of CBH within a window 15 min before and after the analyzed time is required to be less than 30% of mean CBH within the same window. As discussed above, the ASI-pairs and the ASI network are expected to measure a spatial median CBH whereas the ceilometer measures CBH at the point of its installation. This restriction aims to~~
535 ~~assure comparability of both measurements.~~

pp. 28-29, ll. 691-702:

The statistical evaluations are now restricted to times in which the variability of CBH is small. More precisely, the standard deviation of CBH within a window 15 min before and after the analyzed time is required to be less than 30% of mean CBH

within the same window. As discussed above, the ASI-pairs and the ASI network are expected to measure a spatial median CBH whereas the ceilometer measures CBH at the point of its installation. This restriction aims to assure a good comparability
695 of both measurements. Further, this way our results are more comparable to a prior study by Kuhn et al. (2019).

Accuracies of CBH measurement by ASI-pairs and ASI network are analyzed separately for five ranges of reference CBH defined by the bounds $\{0, 1, 2, 4, 8, 12\}$ km. The number of CBH measurements included in this evaluation is given in Table 1 for each of these ranges. The interval bounds are spaced irregularly to correspond better to the distribution of CBH at the site (see also Fig. 4). Table 1 also shows the number of observations excluded from the validation as significant temporal variability
700 of CBH was detected for these observations. While a significant fraction of the readings is sorted out, the representation of the CBH ranges remains widely comparable to the original data set (see Fig. 2, left). Only the range of lowest CBH < 1000 m is represented by a notably smaller share of the validation data set.

p. 28, Table 1:

Table 1. Frequency of measurements from the validation data set (period 30 June 2019 to 27 September 2019) per range of cloud base height (CBH) used in the evaluations described in Sect. ~~4~~4.4 (retained) and frequency of those filtered from the evaluation due to increased variability of CBH (rejected).

CBH range [km]	~~Number of observations~~Observations retained	Observations rejected
$0 < \text{CBH} \leq 1$	11844	13255
$1 < \text{CBH} \leq 2$	14130	9120
$2 < \text{CBH} \leq 4$	9962	5923
$4 < \text{CBH} \leq 8$	5559	3570
$8 < \text{CBH} \leq 12$	4935	1355

General comment 4:

Reviewer:

The Authors measure accuracy of their approach by using a three-month dataset, shown in Fig. 9 and elaborated in Section 4.3. From a machine-learning stand point is would be important to know if these were “training samples” (i.e., used to prepare CBH probabilities, etc.) or whether these data points were withheld from algorithm preparation.

Authors’ response:

In the study we use two separate data sets: one for training/development of the method and one for the test/validation. The training period is 01 April 2019 to 29 June 2019. The validation period is 30 June 2019 to 27 September 2019. We hope that this answers the reviewer’s question satisfyingly. We revised passages, by which we intended to describe this split of the used dataset, as shown below, for more clarity.

Changes in manuscript:

p. 20, l. 530:

> In this section, the accuracy of CBH measurement by the ASI network and by 42 independent ASI-pairs set up at a wide variety of camera distances and alignments is compared. This section is based on a validation data set including the days
> 530 from 30 June 2019 to 27 September 2019. This dataset was excluded from the model development described in Sect. 3. The

p. 7, ll. 160-162:

> 160 used for deriving the method (until 29 June 2019) and a period used for validations (starting from 30 June 2019). Time stamps from the validation period 30 June 2019 to 27 September 2019 are excluded from the model development and also from the estimation of conditional probabilities.

General comment 5:

Reviewer:

The Authors introduce the Maximum Likelihood Estimation (MLE) approach in Section3.4 and – before in Section 3.3 – provide information on conditional CBH probability. This arrangement seems confusing to me and recommend that Section 3.3 follows 3.4(or is a subsection of 3.4).

Authors' response:

We changed the order of the sections accordingly. As this change would obscure the markup of other changes in the red-line version, we excluded this exchange from the markup (by applying the change before comparing with latexdiff).

These sections have additionally been revised strongly based on Reviewer Comment 2, Major Comment 1.

Changes in manuscript:

Order of 3.3 and 3.4 is exchanged (p. 12-20, ll. 311-526):

3.3 Estimating CBH in the ASI network (ORDER OF SECTIONS 3.3 AND 3.4 WAS EXCHANGED)

~~The estimation procedure presented here is motivated by~~ In this section we present our method to combine the measurements of CBH from a large number ASI-pairs organized as network. Prior works estimated CBH by a small number of two or in some cases four ASIs (Nouri et al., 2019a). However, with a large number of ASI-pairs, we consider a statistical method promising, which analyzes the CBH samples received and, based on the known characteristics of each ASI-pair, determines

3.4 Estimation of conditional probabilities of CBH (ORDER OF SECTIONS 3.3 AND 3.4 WAS EXCHANGED)

The procedure to combine CBH-measurements from independent ASI-pairs, which are organized as a network, requires knowledge of the (conditional) probability to receive a certain reading of CBH from an ASI-pair given the true CBH takes on some specific value. The ~~method itself will be presented in Sect. 3.3. Here we discuss the probability distributions used. The~~ required

General comment 6:

Reviewer:

Section 3.3 lists a variety of filters that were applied (ll. 240ff). The Authors should revise Section 3.3 and reference the use of these filters - if applied in the past – and explain their intended effect.

Authors' response:

We revised Sect. 3.4 (in new order) strongly according to the reviewer's feedback but also based on the Reviewer Comment 2, Major Comment 1. We now pointed out, why a method to estimate the distributions of conditional probability from measurement data, was developed, which was new in our perspective at least to this application. Such distributions were so far not available for stereoscopic CBH measurements.

We moved details on the implementation of the filters to the appendix and focused on the intended effects of the filters and motivated the value assigned to the parameters of the filters.

Changes in manuscript:

pp. 16-20, ll. 403-526

3.4 Estimation of conditional probabilities of CBH (ORDER OF SECTIONS 3.3 AND 3.4 WAS EXCHANGED)

The procedure to combine CBH-measurements from independent ASI-pairs, which are organized as a network, requires knowledge of the (conditional) probability to receive a certain reading of CBH from an ASI-pair given the true CBH takes on some specific value. The ~~method itself will be presented in Sect. 3.3. Here we discuss the probability distributions used. The~~ required distribution aims to answer the following question: If true CBH ranges in between 1.8...1.9 km, how large will be the probability that an ASI-pair with camera distance 2.2 km delivers a certain CBH e.g. within 0...0.1 km or 1.8...1.9 km or 11.9...12 km? In the following, these conditional probabilities are estimated not only for the range of true CBH between 1.8...1.9 km but

times ~~, we aim to suppress~~ (such as represented by the validation data set). To suppress such random features of received joint frequency distributions~~. For this , the original joint frequency distribution F_l of ASI-pair l is transformed by a first filter into $F_{l,filter\ 1}$ and by a consecutively applied filter into $F_{l,filter\ 2}$.~~, we introduce a filtering procedure with two consecutive steps described here and in more detail in Appendix A. The parameter values set in the filtering procedure are approximate to this point and are based on a visual comparison of unfiltered and filtered distributions, evaluating the degree to which noise but also reasonable features were suppressed. The parameters values may be optimized in a future study.

First, a weighted mean filter is applied between the original joint frequency distributions ~~F_l received from all~~ received for ASI-pairs with ~~arbitrary camera distance d~~

$$F_{l,filter\ 1} = \frac{\sum_j w_{l,m} F_m}{\sum_j w_{l,m}}.$$

~~For the joint frequency distribution F_l of each respective ASI-pair l, weights $w_{l,m}$ are used that include~~ similar camera distance. As discussed above, ASI-pairs with similar camera distance ~~. More precisely, a triangular window, based on the difference of camera distance $\Delta d_{l,m}$ of ASI-pair m compared to ASI-pair l, is used that is defined by~~

$$w_{l,m} = max(0, 1 - \Delta d_{l,m}/0.5\ \mathrm{km}).$$

~~Then~~ are expected to perform similarly in the measurement of CBH and should consequently also exhibit similar joint frequency distributions of CBH. Thus, the filter aims to suppress differences between the joint frequency distributions of ASI-pairs which may result from disturbances in the estimation rather than from a difference in the systems' characteristics.

To each filtered distribution resulting from the prior step, a composite of three Gaussian filters is applied~~to $F_{l,filter\ 1}$ of each ASI-pair l~~. We first decompose each distribution ~~$F_{l,filter\ 1}$~~ by conditional filters into three separate *modes*~~. In the second step~~, which correspond to parts of the joint frequency distributions which are estimated with descending precision. Thereafter, we apply ~~to each mode~~ a Gaussian filter ~~g_σ with distinct standard deviation σ_{mode}~~ to each mode. The standard deviation of the Gaussian ~~kernel. The subscript *mode* indicates the specific mode for which σ_{mode} is applied.~~ filter applied to each mode corresponds qualitatively to the uncertainty with which the prior joint frequency distribution is estimated within grid cells of that mode. Consecutively, the three filtered modes are summed to receive the smoothened joint frequency distribution.

The first mode is constituted by ~~all outlier observations. Outliers are defined here as grid cells (h_{Ref}, h_{ASI}) for which~~ grid cells for which the ASI-pair based measurement of CBH ~~h_{ASI}~~ deviates by more than 1.5 km from the ceilometer reading~~h_{Ref}~~:

$$F_{l,outlier}(h_{Ref}, h_{ASI}) = \begin{cases} F_{l,filter\ 1}(h_{Ref}, h_{ASI}), & |h_{ASI} - h_{Ref}| > 1.5\ \mathrm{km} \\ 0, & \text{else.} \end{cases}$$

~~Such outliers will contain a large random component. We expect that in a reproduction of the experiment, a similar number of outliers will be received, while~~ . The large deviations represented by this mode occur less frequently which is why the joint frequency distribution will be estimated less precisely for the respective grid cells. On the other hand, apart from such

scattering effects, the joint frequency ~~found for a single grid cell (h_{Ref}, h_{ASI}) may vary significantly. Therefore, the strongest filter~~ distributions are found to be comparably smooth in the grid cells of this mode. A Gaussian filter with a large standard deviation of 1 km is applied to this mode ~~using $\sigma_{outlier} = 1$ km.~~ which is considered to be apt to preserve the expected distribution while suppressing random features.

The second mode is constituted by grid cells ~~that are not part of the first mode and~~ for which the ASI-pair based measurement of CBH deviates by less than 1.5 km from the ceilometer reading and which feature a joint frequency ~~less than the average over~~ below the average of all grid cells~~of the joint frequencydistribution:~~

$$F_{l,inconfident}(h_{Ref}, h_{ASI}) = \begin{cases} F_{l,filter\ 1}(h_{Ref}, h_{ASI}), & |h_{ASI} - h_{Ref}| \leq 1.5 \text{ km} \\ & \wedge\ F_{l,filter\ 1}(h_{Ref}, h_{ASI}) < \text{mean}(F_{l,filter\ 1}) \\ 0, & \text{else.} \end{cases}$$

~~The~~ . These grid cells typically exhibit a larger joint frequency, i.e. more observations, than grid cells in the first mode. Still the comparably small number of observations in these grid cells is expected to cause an increased uncertainty of the estimated joint frequencies. ~~For this mode, $\sigma_{inconfident} = 0.5$ km~~ Consequently in a trade-off between suppressing random scattering and preserving meaningful variations a Gaussian filter with standard deviation 0.5 km is applied.

The third mode ~~$F_{l,confident}(h_{Ref}, h_{ASI})$~~ makes up the complementary of the first and second mode. It contains grid cells that are observed with an at least average joint frequency and which are not classified as outliers~~:~~

$$F_{l,confident}(h_{Ref}, h_{ASI}) = \begin{cases} F_{l,filter\ 1}(h_{Ref}, h_{ASI}), & |h_{ASI} - h_{Ref}| \leq 1.5 \text{ km} \\ & \wedge\ F_{l,filter\ 1}(h_{Ref}, h_{ASI}) \geq \text{mean}(F_{l,filter\ 1}) \\ 0, & \text{else.} \end{cases}$$

. Joint frequencies in these grid cells are considered to ~~have~~ be estimated with a comparably high accuracy. To avoid a loss of precision and ultimately a loss of accuracy in the estimation of CBH, a ~~small value of $\sigma_{confident} = 0.1$ km~~ Gaussian filter with a standard deviation of 0.1 km is used. ~~The three filtered modes g_σ are summed to receive the smoothened joint frequency distribution~~

$$F_{l,filter\ 2} = g_{\sigma_{outlier}}(F_{l,outlier}) + g_{\sigma_{inconfident}}(F_{l,inconfident}) + g_{\sigma_{confident}}(F_{l,confident}).$$

Hence, only neighboring grid cells have a significant influence on this filter.

In many joint frequency distributions, there are grid cells with joint frequency close to zero. Especially for these grid cells, a greater ~~dataset~~ data set would be required to receive more representative values. For all grid cells, joint frequency is increased to a minimum value of 0.5 to avoid underestimations of joint frequency. This value corresponds to half of the joint frequency associated with a single actual observation in a grid-cell. For the estimation procedure of CBH, ~~this~~ such a minimum value leads to slightly reduced precision for most readings but increased robustness in the case that these grid cells (h_{Ref}, h_{ASI}) are indeed observed in the measurement.

~~Finally,~~ Finally, from each joint frequency distribution~~is normalized with the sum of all joint frequency grid cells. In this way, a probability mass function (also known as discrete density function) to measure a certain CBH with the respective ASI-pair and to coincidentally measure a certain CBH with the ceilometer is yielded. The~~ , the conditional probability $P(h_{ASI} \mid h_{Ref})$ to receive a certain CBH reading from an ASI-pair, given that the ceilometer measures some certain CBH, is ~~calculated by dividing the respective probability mass function by the marginal distribution of CBH measured by the ceilometer. The latter distribution gives the probability to receive CBH from the ceilometer within a certain bin h_{Ref} regardless of which CBH reading is simultaneously received from an ASI-pair. The distribution can be derived from any of the probability mass functions by summing all grid cells of the probability mass function which correspond to the respective bin h_{Ref} of CBH measured by the ceilometer.~~ derived (see Appendix A for a more detailed description).

~~Inference procedure — Step 1: For each range i of camera distance CBH$_i$ is computed as mean CBH from the respective ASI-pairs. Conditional probability is evaluated that CBH$_i$ would be received if true CBH (at the ceilometer) took on a value {0...0.1,0.1...0.2,...,11.9...12} (red boxes). Step 1 yields a likelihood function for each range of camera distance. Step 2: Cumulative and complementary cumulative likelihood are calculated for each range of camera distance. Step 3: These functions are logarithmized and then summed over all ranges i of camera distance yielding overall cumulative and complementary cumulative likelihood. Step 4: The Intersection of both functions gives the estimated likeliest CBH.~~

The inference procedure, which ~~is~~ was introduced in Sect. 3.3, represents each range i of camera distance bounded by the limits $\{0.5, 1, 1.5, ..., 6\}$ km by a single distribution of conditional probability. For each range of camera distance, the distribution of conditional probability, which corresponds to the camera distance closest to the center of this range, is selected ~~. For example , for the range $i = 2$ representing camera distances 1...1.5 km, the center of the range would be 1.25 km. For the camera distances 1.081, 1.247 and 1.352 km, conditional probabilities have been modeled. Consequently, for this range of camera distance, the distribution of conditional probability corresponding to the camera distance 1.247 km is used.~~ (example provided in Appendix A). Figure 5 (above Step 1) shows exemplary conditional probabilities for three ASI-pairs with camera distances 0.8, 2.2, 5.7 km representing the ranges of camera distance $i = 1,\ 4,\ 11$ respectively. ~~The further content of Fig. 5 is explained in the next section~~BIAS and precision, with which ASI pairs of distinct camera distances measure CBH, given a certain reference CBH, are visible in these conditional probabilities. Such characteristics will be evaluated in more detail in the following, based on a separate validation data set.

Appendix A, pp. 35-37:

Appendix A: Details on the retrieval of conditional probabilities

A1 Retrieval of raw joint frequency distributions

CBH from the respective ASI-pair and from the ceilometer are processed by a moving-median filter with a window of 10 min. The joint frequency distribution of CBH measured by ceilometer h_{Ref} and the respective ASI-pair h_{ASI} is computed from these simultaneously acquired time series. That means, the frequency is calculated with which (h_{Ref}, h_{ASI}) is observed in a discrete grid cell defined by the interval $[j\Delta h, (j+1)\Delta h[$ for h_{Ref} and the interval $[k\Delta h, (k+1)\Delta h[$ for h_{ASI}, where $j, k \in \{0, 1, 2, ..., N-1\}$, where N is the number of bins used for CBH in the analysis. A bin size $\Delta h = 100$ m is chosen in a trade-off between sources of error. Finer bins will allow to represent the distributions at higher resolution and will thus allow for higher resolved measurements of CBH in the network. However, the size of the used data set is limited which makes it difficult to model these distributions at highest resolution. The bin size chosen here is expected to limit the achievable uncertainty of the measurement to a minimum level of 100 m. Joint frequency distributions modeled here are restricted to a maximum CBH of 12 km. This yields $N = 120$.

A2 Filtering operations applied

First, a weighted mean filter is applied between original joint frequency distributions F_l received from all ASI-pairs with camera distance d, this yields $F_{l,filter\ 1}$:

$$F_{l,filter\ 1} = \frac{\sum_m w_{l,m} F_m}{\sum_m w_{l,m}}. \tag{A1}$$

For the joint frequency distribution F_l of each respective ASI-pair l, weights $w_{l,m}$ are used that include ASI-pairs with similar camera distance. More precisely, a triangular window, based on the difference of camera distance $\Delta d_{l,m}$ of ASI-pair m compared to ASI-pair l, is used that is defined by

$$w_{l,m} = max(0, 1 - \Delta d_{l,m}/0.5\ \mathrm{km}). \tag{A2}$$

We decompose each distribution $F_{l,filter\ 1}$ by conditional filters into three separate *modes*. In the second step, we apply to each mode a Gaussian filter g_σ with distinct standard deviation σ_{mode} of the Gaussian kernel. The subscript *mode* indicates the specific mode for which σ_{mode} is applied. The first mode is constituted by all outlier observations. Outliers are defined here as grid cells (h_{Ref}, h_{ASI}) for which ASI-pair measurement of CBH h_{ASI} deviates by more than 1.5 km from the ceilometer reading h_{Ref}:

$$F_{l,outlier}(h_{Ref}, h_{ASI}) = \begin{cases} F_{l,filter\ 1}(h_{Ref}, h_{ASI}), & |h_{ASI} - h_{Ref}| > 1.5\ \mathrm{km} \\ 0, & \text{else.} \end{cases} \tag{A3}$$

Such outliers will contain a large random component. We expect that in a reproduction of the experiment, a similar number of outliers will be received, while the joint frequency found for a single grid cell (h_{Ref}, h_{ASI}) may vary significantly. Therefore, the strongest filter is applied to this mode using $\sigma_{outlier} = 1$ km.

The second mode is constituted by grid cells that are not part of the first mode and feature a joint frequency less than the average over all grid cells of the joint frequency distribution:

$$F_{l,inconfident}(h_{Ref}, h_{ASI}) = \begin{cases} F_{l,filter\ 1}(h_{Ref}, h_{ASI}), & |h_{ASI} - h_{Ref}| \leq 1.5\ \mathrm{km} \\ & \wedge\ F_{l,filter\ 1}(h_{Ref}, h_{ASI}) < \mathrm{mean}(F_{l,filter\ 1}) \\ 0, & \text{else.} \end{cases} \tag{A4}$$

The comparably small number of observations in these grid cells is expected to cause an increased uncertainty of the estimated joint frequencies. For this mode, $\sigma_{inconfident} = 0.5$ km is applied.

General comment 7:

Reviewer:

The Authors list high temporal and spatial resolutions (“30 s or 5 m”, l. 6) of state-of-the-art nowcasts. It is not obvious if chosen CBH intervals (“100m”, l. 231) are fine enough to provide such high resolution. Perhaps the Authors could expand on this in Section 3.3 or in their discussion to address this question.

Authors’ response:

We agree with the reviewer that indeed the specification of the used state-of-the-art ASI-pairs may appear contradictory to the accuracy of the CBH estimation attested in this study for all of the studied ASI-based CBH measurements. As suggested, we added a short discussion to give an

explanation why ASI-based nowcasts may be provided at a resolution which is by far finer than the deviations of cloud shadow positions induced by deviations in the estimation of CBH. The source cited in this discussion was additionally added to the introduction. Note that Sect. 4.4 was also reworked based on Reviewer Comment 2, Major Comment 2.

Changes in manuscript:

p. 2, ll. 37-38:

nowcasts can reduce the uncertainty of supply from solar power plants and can support efficient balancing of energy supply and demand (Law et al., 2014; Kaur et al., 2016). Further, they can be applied to control concentrating solar power plants (Nouri et al., 2020a) more efficiently. The coordination of renewable production and energy consumption at a local scale is a way to minimize requirements on grid-infrastructure while keeping curtailment of feed-ins from renewable sources at a low level. Ghosh et al. (2016) use nowcasts (15 s ahead) to control PV-feed in and provide reactive power. In this context, spatially

p. 30, ll. 740-754:

~~statistics and from an inspection of the ASI images observations of higher CBH layers are likely to be found in the presence of a lower layer. As discussed in Sect. 3.1 the~~ ASI-based estimation of CBH in this study. Meanwhile, the underlying ASI-pairs ~~measure CBH of the most dominant cloud layer in the sense of optical thickness and area in the analyzed field of view of the sky. When for example, a CBH of 10 km is present the corresponding spatial area included has side lengths of 15.7 km. For multi-cloud-layer conditions it is likely that within this window lower clouds are present which are recognized by an ASI-pair instead.More aggressive filtering of such multilayer situations included in the evaluation could reduce this influence but would further limit the database. The distance between the cameras used by an ASI-pair and the reference ceilometer are not found to have a significant influence on received accuracy in the evaluated data set. This was expected in part from the previously discussed effect that the~~ can nowcast 30 s-averages of solar irradiance at a spatial resolution of 5 m × 5 m. According to the considerations of Nouri et al. (2019b) and with the sun elevations occuring at the site, deviations in CBH may cause deviations in the positions of cloud shadow edges of at least 100 m under favorable conditions for the ASI-pairs ~~measure CBH of the most dominant cloud layer~~and also for the ASI-network. This deviation is much larger than the spatial resolution of these maps of solar irradiance. For certain applications, e.g. to control solar power plants (Nouri et al., 2020a), it may still be advantageous to provide maps of solar irradiance at a resolution finer than the uncertainty of cloud shadow edge positions, as the statistical properties of spatial variability may still be captured in these maps.

General comment 8:

Reviewer:

To help the reader appreciate the scientific advance in the work, the Authors should stress wherever (in Section 3.3 or 3.4) new techniques were developed or combined.

Authors' response:

To emphasize the novelty of the method used in the study we added a short introduction to the MLE-based method in 3.4. Our combination method allows to combine the CBH measurements from a large number of ASI-pairs. Additionally, the method takes account of the individual characteristics of

the ASI-pairs by the use of conditional probabilities. Finally, the use of MLE is to the best of our knowledge not known to this application.

Further we also pointed out that the required distributions of conditional probability were so far not available for CBH measurement by ASI-pairs.

Changes in manuscript:

pp. 12-13, ll. 312-321:

~~The estimation procedure presented here is motivated by~~ In this section we present our method to combine the measurements of CBH from a large number ASI-pairs organized as network. Prior works estimated CBH by a small number of two or in some cases four ASIs (Nouri et al., 2019a). However, with a large number of ASI-pairs, we consider a statistical method promising, which analyzes the CBH samples received and, based on the known characteristics of each ASI-pair, determines the CBH which is most likely to be present. The characteristics of each ASI-pair are in the following described by conditional probability distributions, which will by retrieved in Sect. 3.4. These distributions provide the probability of receiving a certain CBH reading from an ASI-pair, given that actually a specific reference CBH is present. Our estimation procedure then uses principles from Maximum Likelihood Estimation (MLE) ~~. Figure~~and modifies them for the specific case. To the best of our knowledge, the usage of a statistical method and in particular one relying on conditional probability distributions is novel to the task of estimating CBH from the observations of a multitude of ASIs.

p. 17, ll. 409-410:

for each range $\{0...0.1, 0.1...0.2, 0.2...0.3, ..., 11.9...12\}$ km of true CBH. Conditional probability distributions of this kind are not available so far for ASI-pairs. Therefore, we aim to approximate them from the measurement data of a modelling period. Estimations of CBH from the available ASI-pairs and measurements from the ceilometer during the period 01 April 2019 to

Minor comment 1:

Reviewer:

Fig. 2: The plot seems to contain redundant information (by switching perspectives between two ASIs). The Authors could color code each perspective or exclude one redundant half.

Authors' response:

We adapted Fig 2 (left) and for consistency also Fig. 2 (right). As suggested, the plots now make it clearer which ASI-pairs' axes orientations and also distances were yielded by switching the used main camera.

Changes in manuscript:

p. 6, Fig. 2:

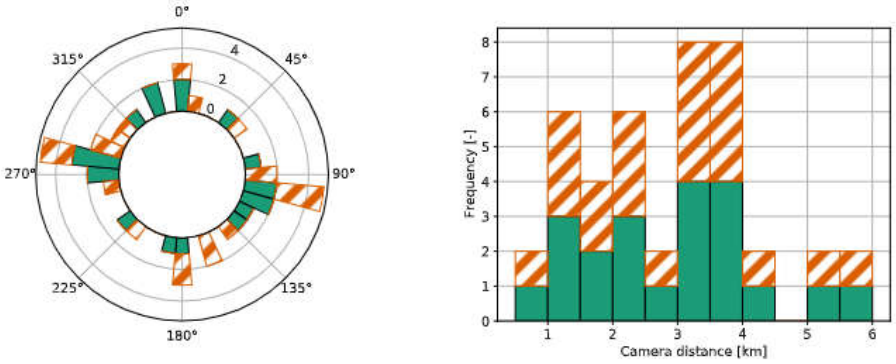

Figure 2. Frequency distribution of ~~camera axis~~ the bearing angles of the ASI-pairs' axes in the set of available ASI-pairs (over north, left) and of available camera distances (right) resulting when arranging the seven ASIs in the urban area into 42 ASI-pairs (from each ~~ASI-tuple~~ 2-ASI-tuple two different ASI-pairs result by switching the main camera, counts of ASI-pairs with switched main camera are marked orange, striped)

Minor comment 2:

Reviewer:

ll. 140-144: Please provide the minimum optical thickness for ceilometer detection.

Authors' response:

We requested this information from the manufacturer but did not receive a response yet. As requested by Reviewer Comment 2, Specific Comment 4, 9, we added a more detailed description of the algorithm used by the ceilometer and extended the description of how this reference instrument was validated in previous studies. We hope that this may be helpful to a possible reader. Otherwise, we hope that we can add this information in a response to be handed in later.

Changes in manuscript:

p. 6, ll. 137-141:

The used ceilometer ~~is~~ of type Lufft CHM 15 k Nimbus ~~.~~ (firmware v0.747) is operated by DLR since 2018. CBH is measured by the manufacturer's *Sky Condition Algorithm* (Lufft, 2018) in the default configuration. Heese et al. (2010) specifies for a ceilometer of the same type, that full overlap of the laser's and the receiver's field of view is reached at a height of 1500 m. However relying on an overlap correction, the manufacturer specifies a minimum CBH of down to 0 m. In this study the manufacturer's default minimum CBH of 45 m is used.

pp. 7-9, ll. 174-203:

Regarding the accuracy of ~~the instrument, a benchmark by Martucci et al. (2010) exhibited a bias~~ ceilometers in general, de Haij et al. (2016) and Görsdorf et al. (2016) noted that there is no generally excepted, quantifiable definition of CBH, yet. Further, due to a lack of reference measurements, benchmarks may typically focus on the consistency of CBH measurements by different types of ceilometers. In a benchmark performed by Martucci et al. (2010), the measurement of a Vaisala CL31 ceilometer CBH_{CL} showed a significant deviation from the reading CBH_{CHM} of the instrument ~~compared to another manufacturer's ceilometer of 160 m. With this in mind, we still consider the instrument to be sufficiently accurate for the scope of this study.~~ used here. This trend was given by $\mathrm{CBH}_{CL} = 160.315\ \mathrm{m} + 0.925 * \mathrm{CBH}_{CHM}$. However, the measurement procedure, of the instrument used here, was modified by firmware updates in the meantime. Görsdorf et al. (2016) presented results from a more recent measurement campaign, CeiLinEx2015, which took place in 2015. In this experiment the measurements of six types of ceilometers were compared. For stratus and stratocumulus clouds as well as for fog, deviations between the instruments of up to 70 m were observed. For each of these conditions, the CHM 15 k, used here, provided the smallest measurements of CBH in terms of mean deviation from the median of all tested instruments. More severe deviations of several kilometers between the instrument types were observed during conditions with heavy rain.

In an acceptance test, de Haij et al. (2016) measured CBH by two CHM 15 k, by a Vaisala LD40 ceilometer, by a UV lidar (Leosphere ALS450) and by visibility sensors mounted in various altitudes on a tower of 213 m height. For CBH of up to 200 m, the CHM 15 k typically measured a CBH 30…50 m smaller than the one of the LD40. However, the CHM 15 k was in better agreement with the estimate based on visibility sensors. Görsdorf et al. (2016) and de Haij et al. (2016) suggest, that the negative mean deviation of the CHM 15 k attested by all these studies, for clouds in the range $\mathrm{CBH} < 3$ km, is mostly caused by the manufacturers' algorithms to detect CBH from backscatter profiles. Whereas, according to the manufacturer (Lufft, 2018), the CHM 15 k detects the rising edge of a backscatter peak that exceeds a threshold, other manufacturers' devices may rather recognize the peak's maximum.

For the range of CBH in 3…12 km, an inspection of timeseries depicted by de Haij et al. (2016) indicates very good agreement of the measurements from CHM 15 k and the UV lidar, used there. As a further test of de Haij et al. (2016), performed at a resolution of 60 s, high clouds, detected by the UV lidar in a range of 6…7.5 km, were to be detected by the CHM 15 k within a tolerance of ±3 classes in hh code (WMO Table 1677). This tolerance corresponds to a CBH-range of ±1050 m centered around the discretized reference CBH. CHM 15 k was attested a probability of detection of $> 98\%$ and a false alarm rate of 0%. Based on these studies, the accuracy of the reference instrument is expected to be adequate for the range of $\mathrm{CBH} < 3$ km and also for the range of $\mathrm{CBH} \geq 3$ km, a rather good performance of the instrument is indicated. The experimental results of this study will in particular be compared to prior studies which used a ceilometer of the same type. This is expected to avoid possible inconsistencies related to the used reference.

Minor comment 3:

Reviewer:

ll. 145-151: Is there a maximum solar zenith angle that limits CBH retrieval?

Authors' response:

The measurement of CBH by the ASI-pairs is in principle only limited by the illuminance of the scene. In this study we included zenith angles smaller than 90 degree. We added a description on this. Note that a further addition was made here based on Reviewer Comment 2, Specific comment 6.

Changes in manuscript:

p. 7, ll. 157-158:

155 avoiding redundant calculations. In this way, computational cost scales mostly linear with the number of ASIs used instead of with the number of ASI combinations so that execution in real time is possible. In total, including computation time, the estimation of CBH by the ASI network can be retrieved within 10 s after image acquisition. CBH is computed by the ASI-pairs and by the ASI network during daytime, i.e. if the sun elevation at the time of image acquisition is greater than 0°.

Minor comment 4:

Reviewer:

l. 171-173: Please substitute “most dominant in features, driven by area and optical thickness” instead of “most dominant in the sense of area and optical thickness”.

Authors’ response:

We appreciate the reviewer’s suggestion and replaced the term accordingly.

Changes in manuscript:

p. 11, ll. 270-271:

270 measurement approximates the median CBH of the cloud layer that is locally most dominant in ~~the sense of~~ features, driven by area and optical thickness.

Minor comment 5:

Reviewer:

l. 193-195: Please link to reference or plot(s) or else put “not shown”.

Authors’ response:

We added this note as suggested.

Changes in manuscript:

p.12, l. 292:

290 Within the range of high clouds, a roll-off of the frequency is seen for CBH > 10 km. A reliable estimation of CBH should therefore provide accurate readings for the range of CBH $\in]0, 12[$ km.

A visual analysis and a k-means classification for the site of Oldenburg (not shown) suggested that local conditions predom-

Minor comment 6:

Reviewer:

Equ. 1: What is "j"?

Authors' response:

We would like to apologize for the mistake, the letter was indeed not intended. We corrected the equation.

Changes in manuscript:

Appendix, p. 36, l. 895:

First, a weighted mean filter is applied between original joint frequency distributions F_l received from all ASI-pairs with camera distance d, this yields $F_{l,filter\,1}$:

895 $$F_{l,filter\,1} = \frac{\sum_m w_{l,m} F_m}{\sum_m w_{l,m}}. \quad \text{(A1)}$$

For the joint frequency distribution F_l of each respective ASI-pair l, weights $w_{l,m}$ are used that include ASI-pairs with similar

Minor comment 7:

Reviewer:

Fig. 8: Please provide performance metrics (e.g., correlation coefficient, bias, and RMSD) to each panel.

Authors' response:

We added performance metrics to all scatter-density plots shown in the publication. We further adapted the scatter-density plots as Sect. 4 was reworked based on Reviewer Comment 2, Major Comment 2.

Changes in manuscript:

p. 24, Fig. 8:

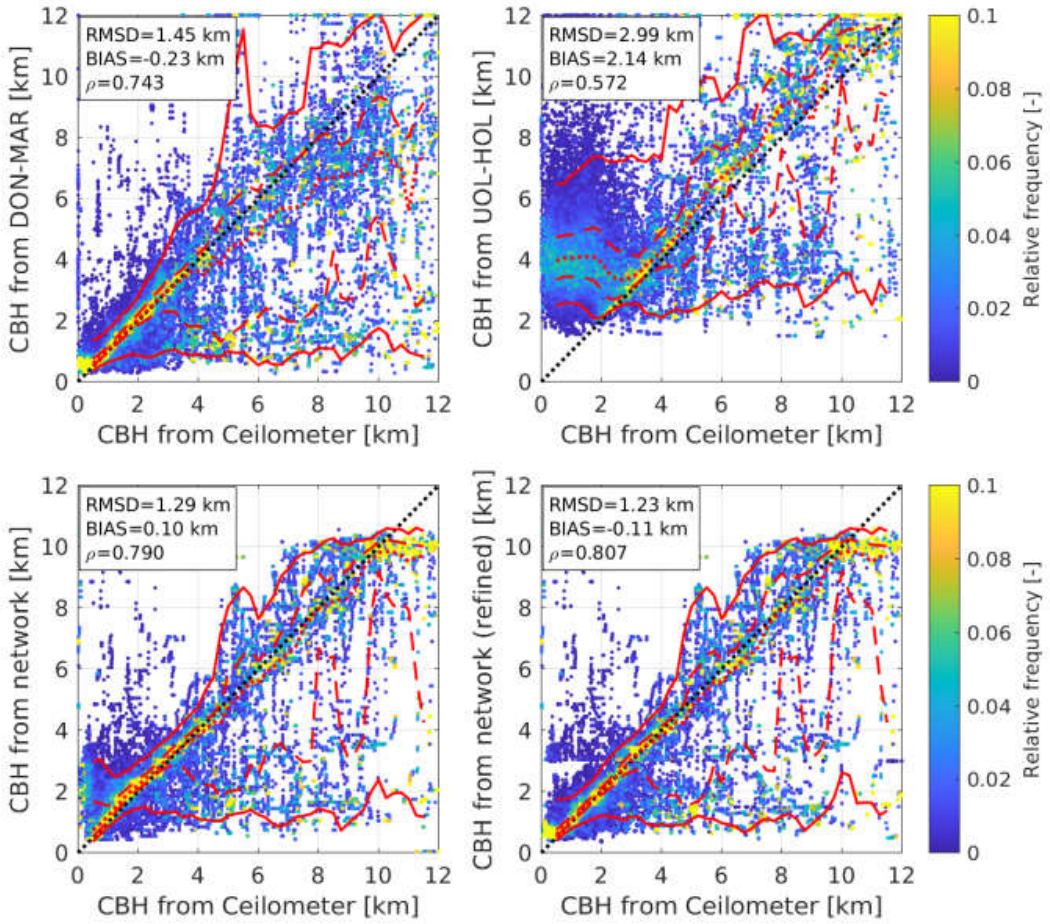

Figure 8. Relative frequency of ASI-based CBH estimation for given CBH from ceilometer. Evaluation for two of the ASI-pairs DON-MAR (upper row, left) and UOL-HOL (upper row, right) with respective camera distances of 0.8 and 5.7 km, and from the ASI network without (bottom row, left) and with refinements (bottom row, right). Relative frequency in each column adds up to 1. Additionally, median (50%-quartile, red dotted), limits to the interquartile range (IQR, red dashed) and 5−95−percentiles (red solid line) based on floating 1000 m-bins of CBH from ceilometer are plotted.